kcal/mol is supported by thermal degradation experiments, which are found to proceed in two stages: an initial stage characterized by low U (~25 kcal/mol) and accounting for 1–10% weight loss, and a second stage for the remaining part which degrades with higher U (~55 kcal/mol) (see: Regel, V. R.; Amelin, A. V.; Pozdnyakov, O. F.; Sanfirova, T. P.; Ioffe, A. F. *Int. Symp. Macromol. 1972*, Helsinki, Finland, July 2–7, 1972, *5*, 163). That initial stage of the degradation process has been explained by the existence of weak links in the polymer, which, in turn, determine its mechanical properties.
(11) Termonia, Y.; Smith, P. in preparation.
(12) Smith, T. L. *J. Polym. Sci.* **1958**, *32*, 99; *SPE J.* **1960**, *16*, 1211.
(13) Bueche, F. *J. Appl. Phys.* **1955**, *26*, 1133.
(14) Bueche, F.; Halpin, J. C. *J. Appl. Phys.* **1964**, *35*, 36.
(15) Vincent, P. I. In "Encyclopedia of Polymer Science and Technology"; Wiley: New York, 1967; Vol. 7, p 292.
(16) Capaccio, G.; Gibson, A. G.; Ward, I. M. In "Ultra-High Modulus Polymers"; Ciferri, A., Ward, I. M., Eds.; Applied Science: London, 1979; p 58.
(17) Barham, P. J.; Keller, A. *J. Polym. Sci., Polym. Lett. Ed.* **1979**, *17*, 591.

Comparison of Experiment and the Proposed General Linear Viscoelastic Theory. 2. Stress Relaxation Line Shape Analysis

Y.-H. Lin

Exxon Chemical Company, Plastics Technology Center, Baytown, Texas 77522.
Received March 26, 1985

ABSTRACT: For testing the proposed general linear viscoelastic theory, the molecular weight (MW) range of the studied samples is extended to as low as $1.24M_e$, overlapping the previous MW range from $13M_e$ to $31M_e$. It is found that the proposed general theory describes quantitatively the linear viscoelastic relaxation spectra over the entire MW range that has been studied. The conclusions about the $\mu_X(t)$, $\mu_B(t)$, and $\mu_C(t)$ processes made in paper 1 are further confirmed. Especially, the theory explains why and how the modulus plateau gradually disappears with decreasing MW. From the spectrum line shape analysis in the $\mu_A(t)$ region, a very significant phenomenon is discovered: With decreasing MW, the friction coefficient for the polymer chain segment to move in the direction perpendicular to the chain contour decreases and converges to the friction coefficient value along the chain contour, which is independent of MW. The effect is attributed to the anisotropic distribution of free volume on the polymer chain—i.e., more free volume at the polymer chain ends than in the interior portion of the chain.

I. Introduction

The effect of chain entanglement on polymer viscoelastic behavior has been an important research subject of polymer physics.[1,2] The concept of chain entanglement started more than half a century ago. Not until the introduction of the idea of reptation by de Gennes[3] to account for the constraint effect of entanglement was it possible to describe the dynamics of long polymer chains in concentrated systems in a meaningful way. In 1978, Doi and Edwards[4-7] recognized the important relation of the reptation motion and the mechanical properties of a concentrated system and derived a rheological constitutive equation. Their theory has successfully explained many characteristic features of viscoelasticity of concentrated polymer systems.

The Doi–Edwards theory mainly dealt with the polymer dynamics and viscoelastic behavior in the terminal region. In the previous report (referred to as paper 1 below),[8] it was theoretically shown how four modes of polymer molecular dynamics affected the linear viscoelasticity of flexible linear polymers. The four dynamic modes $\mu_A(t)$, $\mu_X(t)$, $\mu_B(t)$, and $\mu_C(t)$ are respectively the Rouse chain motion between two adjacent cross-linked points (assuming entanglement points fixed), the chain slippage through entanglement links, the primitive chain-length fluctuation, and the reptational motion corrected for the chain-length fluctuation effect. A general stress relaxation function containing all these dynamic modes was obtained. It was shown that the theory is universal as we normalize molecular weight (MW) with respect to the entanglement MW, M_e, which can be determined from the plateau modulus.

The theory was used to analyze the stress relaxation line shapes of three polystyrene samples of very narrow MWD and of MW's ranging from 186 000 to 775 000. Consistent good agreements between theory and experimental results were obtained. The theory also explained the MW dependence of the zero-shear viscosity ($\eta_0 \propto M^{3.4}$ for $M > M_c$ and $\eta_0 \propto M$ for $M < M_c$) and the steady-state compliance J_e.

Experimentally, the stress relaxation modulus does not show a clear plateau region in the medium and low-MW range ($<8M_e$). Analyzing the stress relaxation line shape in this MW region is a very critical and important test of the theory, even though the theory has predicted the MW dependence of the first and second moments of the relaxation time spectrum (i.e., η_0 and J_e).

Here, a series of polystyrene samples of very narrow MWD and of MW's ranging from 422 000 to 16 700 ($31M_e$–$1.24M_e$) have been studied. The measured stress relaxation line shapes are uniquely quantitatively described by the proposed general linear viscoelastic theory. The conclusions about the $\mu_X(t)$, $\mu_B(t)$, and $\mu_C(t)$ processes made in paper 1 are further confirmed. The prominent role played by the $\mu_B(t)$ mode of motion in the medium and low-MW region is clearly demonstrated. The theoretical analysis of the experimental results shows why and how the modulus plateau gradually disappears with decreasing MW.

About the $\mu_A(t)$ process, a very significant phenomenon is discovered in this study: The friction coefficient for a polymer chain segment to move in the direction perpendicular to the chain contour (extracted from the line shape analysis of the $\mu_A(t)$ process) decreases with decreasing MW in the MW region MW < $10M_e$. The ratio of K'/K (i.e., the ratio of the friction coefficients for the polymer chain segment to move perpendicular to vs. along the chain contour) decreases from a plateau value of 3.3 at high MW to a limiting value of 1 at low MW (M_c > MW > M_e), while K is independent of MW. The physical meaning of this phenomenon is explained in terms of the free volume associated with the polymer chain ends.

II. Theory

Following a step-shear deformation and before the

0024-9297/86/2219-0159$01.50/0

Table I

	M_w	M_w/M_n	characterization[a]
F40	422 000	1.05	TSK
NBS	179 000	1.07	NBS
L11	110 000		LF
F10	102 000	1.02	TSK
P7	68 000		PS
P5	51 500		PS
F4	43 900	1.01	TSK
L3	35 100	1.03	LF
P3	34 500		PS
F2	16 700	1.02	TSK

[a] TSK: Toyo Soda Manufacturing Co., Japan, with light scattering, intrinsic viscosity, and GPC methods. NBS: National Bureau of Standards with light scattering and osmometry. PS: Polysciences, Inc. with GPC. LF: L. J. Fetters, Exxon CRSL, with GPC.

polymer chain has a chance to slip through an entanglement link, the stress relaxation of the polymer behaves like that of a cross-linked rubber. Thus, the Rouse chain motion[8,9] between two cross-linked points (or fixed entanglement links), $\mu_A(t)$, is the main stress relaxation mechanism. As the polymer chain slips through the entanglement links to equilibrate segmental density along the chain contour, the modulus (for a simple shear) relaxes from the value G_N', given by

$$G_N' = \frac{3\rho RT}{M_e\lambda}\langle(\mathbf{E}\cdot\mathbf{u})_x(\mathbf{E}\cdot\mathbf{u})_y\rangle \tag{1}$$

to the value G_N, given by

$$G_N = \frac{3\rho RT}{M_e\lambda}\left\langle\frac{(\mathbf{E}\cdot\mathbf{u})_x(\mathbf{E}\cdot\mathbf{u})_y}{|\mathbf{E}\cdot\mathbf{u}|}\right\rangle\Big/\langle|\mathbf{E}\cdot\mathbf{u}|\rangle \tag{2}$$

where $\mathbf{E}$ is the deformation tensor for simple shear

$$\mathbf{E} = \begin{vmatrix} 1 & \lambda & 0 \\ 0 & 1 & 0 \\ 0 & 0 & 1 \end{vmatrix} \tag{3}$$

Equation 1 is from the theory of rubber elasticity,[10,11] and eq 2 was obtained by Doi and Edwards.[5] It has been shown that eq 2 describes the measured damping function in the terminal region very well.[12-14] The particular dynamic mode, $\mu_X(t)$, describing the slippage of the polymer chain through entanglement links is a logical consequence of the shown validity of eq 2. For a simple shear deformation in the linear region, G_N is smaller than G_N' by a factor of $^4/_5$.

After the $\mu_X(t)$ process, the processes that relax the remaining polymer stress are the primitive chain-length fluctuation, $\mu_B(t)$, and the reptational motion corrected for the chain-length fluctuation effect, $\mu_C(t)$. Both these two modes of motions relax the polymer stress by moving the chain end through an entanglement link (i.e., disentanglement). The chain-length fluctuation process relaxes the stress at both tube ends to a length proportional to $(M_e/M)^{1/2}$. The remaining tube length proportional to $1 - (M_e/M)^{1/2}$ is relaxed by the $\mu_C(t)$ process. While the $\mu_C(t)$ process is basically reptational, $\mu_B(t)$ is a Rouse-type process. Although chain length fluctuation and reptational processes proceed simultaneously, the theoretical expressions of $\mu_B(t)$ and $\mu_C(t)$ correspond to two decoupled processes.[8] In the wide MW range, $M > M_C$, the $\mu_C(t)$ process is slower than the $\mu_B(t)$ process. At M_C, the characteristic times of $\mu_B(t)$ and $\mu_C(t)$ cross over.

Including all the four dynamic modes $\mu_A(t)$, $\mu_X(t)$, $\mu_B(t)$, and $\mu_C(t)$, a general functional form for the stress relaxation modulus after a step-shear deformation in the linear region has been derived as[8]

$$G(t) = \frac{4\rho RT}{5M_e}[1 + \mu_A(t/\tau_A)][1 + {}^1/_4\exp(-t/\tau_X)] \times [B\mu_B(t/\tau_B) + C\mu_C(t/\tau_C)] \tag{4}$$

where the notation is the same as in paper 1

$$\mu_A(t/\tau_A) = \sum_P^{N_e-1}\exp(-t/\tau_A{}^P) \tag{5}$$

with

$$\tau_A{}^P = \frac{K\pi^2}{24\sin^2(\pi P/2N_e)}\frac{M_e{}^2}{N_e{}^2} \tag{6}$$

$$B = (M_e/M)^{1/2} \tag{7}$$

$$C = 1 - B \tag{8}$$

$$\mu_B(t/\tau_B) = \sum_{p\ \mathrm{odd}}\frac{8}{\pi^2P^2}\exp(-P^2t/\tau_B) \tag{9}$$

with

$$\tau_B = (1/3)KM^2 \tag{10}$$

and

$$\mu_C(t/\tau_C) = \sum_{p\ \mathrm{odd}}\frac{8}{\pi^2p^2}\exp(-P^2t/\tau_C) \tag{11}$$

with

$$\tau_C = K(M^3/M_e)[1 - (M_e/M)^{1/2}]^2 \tag{12}$$

All the relaxation times in the above equations are proportional to the constant K, given as

$$K = \zeta b^2N_0{}^2/kT\pi^2M^2 \tag{13}$$

In the high-MW region ($>10M_e$), it was found from analyzing the experimental results that the K value in eq 6 (denoted as K' below) was a few times greater than the K value in eq 10 and 12.

Both the static quantities, B and C, are expressed in terms of the reduced MW, M/M_e. As we normalize τ_B and τ_C with respect to $\tau_A{}^1$, the relaxation times are functions of the reduced MW as well. Thus, the theory is universal in terms of the reduced MW. The entanglement MW, M_e, can be determined independently from the plateau modulus, G_N, using the equation

$$M_e = 4\rho RT/5G_N \tag{14}$$

By keeping the universality applicable in the $\mu_X(t)$ region, we obtained by a combination of a scaling argument and analysis of experimental results

$$\tau_X = 0.55KM_eM \tag{15}$$

III. Experiment

Polystyrene samples of very narrow MWD were used for linear viscoelastic measurements in this study. The details of sample preparation have been described before.[12] The measurements were made with the System Four mechanical spectrometer manufactured by Rheometrics, Inc.

Among the polystyrene samples studied, NBS was obtained from the National Bureau of Standards, F40, F10, F4, and F2 from TSK (Toyo Soda Manufacturing Co., Japan), and P7, P5, and P3 from Polysciences, Inc. L11 and L3 were kindly supplied by L. J. Fetters of Exxon Research and Engineering Co. The methods of characterization and the weight-average MW's (M_w) of these samples are listed in Table I.

In this study, the measurements were made with a 10 kg·cm transducer, which is about five times stiffer than the 2 kg·cm transducer used previously. The result of F40 measured with the

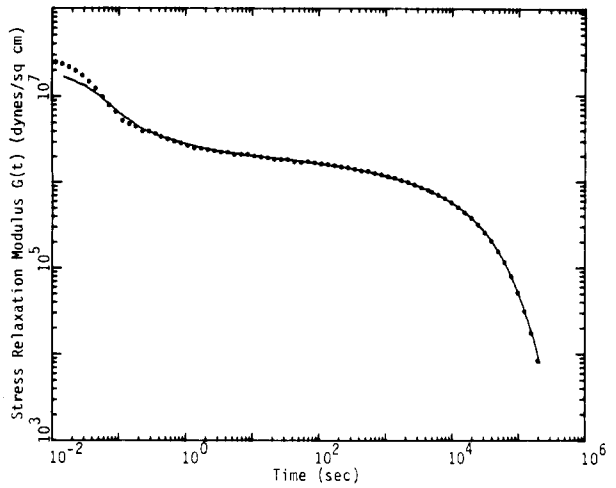

Figure 1. Comparison of the stress relaxation moduli of the F40 sample measured with the 10 kg·cm (···) and 2 kg·cm (—) transducers.

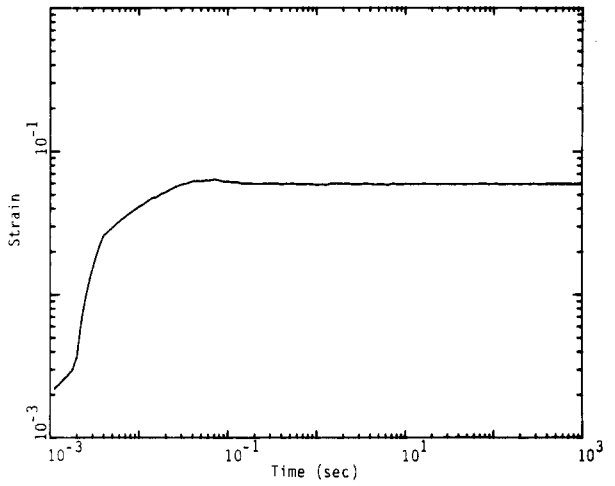

Figure 2. Applied step strain of 0.06 for the stress relaxation measurements.

2 kg·cm transducer and reported previously is compared with the one measured with the 10 kg·cm transducer, as shown in Figure 1. After the glassy region (after 2×10^{-1} s in Figure 1), virtually no difference in line shape is observed between these two results. In this study, we do not attempt to analyze the line shape in the glassy region, which is related to the local segmental motion. Since after the glassy region, the line shape is independent of the stiffness of the transducer, the correction due to the compliance of the transducer should be negligible. This is confirmed by the calculation based on the measured compliance of the transducer.

The System Four mechanical spectrometer is capable of performing a step deformation to a strain of 0.06, as shown in Figure 2, which is used in the linear viscoelastic relaxation measurements in this study. The step deformation reaches the fixed plateau value at about 40×10^{-3} s. Thus, for the time region of stress relaxation of our present interest (i.e., after 0.2 s), the step deformation rising time is sufficiently short.

When oscillatory measurements for storage and loss moduli are made, both the strain signal of the servo system and the stress signal from the transducer are correlated with a standard sine wave to calculate the in-phase and out-of-phase modulus components. Because of these correlation steps, the obtained modulus values should be more reliable than the stress relaxation measurements. To confirm the measurements and line shape analysis of $G(t)$, the storage and loss moduli of F10, P7, P5, F4, and F2 were measured.

IV. Stress Relaxation Modulus

1. Experimental Results. The measured stress relaxation curves of different MW's at 127.5 ± 0.5 °C are shown in Figure 3. At high MW, a plateau region is clearly

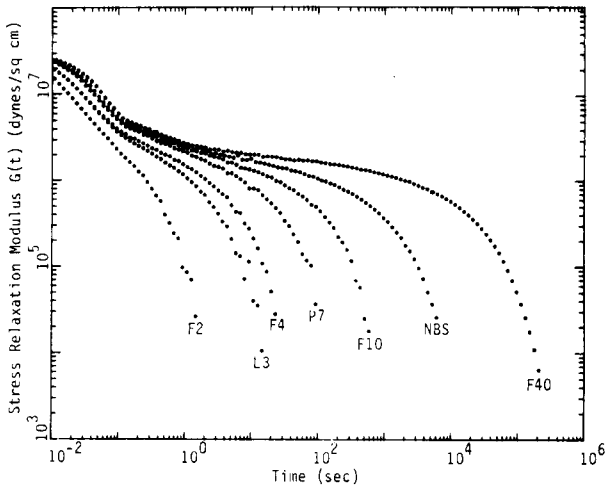

Figure 3. Comparison of the measured stress relaxation moduli of F40, NBS, F10, P7, F4, L3, and F2.

noticeable. As the MW decreases, the plateau gradually disappears. The phenomenon has been observed in the measurements of the storage and loss moduli and was well documented in literature.[1,2,15]

In the glassy and transition regions, the stress relaxation curves shift to shorter times as the MW decreases. This has to do with the change of the glass transition point, T_g, or free volume in the polymer melt with MW.[16]

2. Line Shape Analysis. The terminal relaxation time is highly sensitive to MW; it was shown that MWD need to be considered in analyzing the stress relaxation line shape.[8,12] In this study, one of our main interests is to analyze the stress relaxation in the MW region where the modulus plateau is greatly reduced. In this MW region, because the relaxation times of the different dynamic modes (i.e., $\mu_X(t)$, $\mu_B(t)$, and $\mu_C(t)$) are close to each other, it is difficult to do the nonlinear least-squares fitting of the measured line shape to the theoretical form to obtain the MWD of the sample as done previously. Instead, we assume that the very narrow MWD of all the studied samples except NBS and F40 can basically be described by the Schulz MWD[17,18]

$$W(M) = \frac{Z^{Z+1}}{\Gamma(Z+1)}\left(\frac{M}{M_n}\right)^Z \frac{1}{M_n} \exp\left(\frac{-ZM}{M_n}\right) \quad (16)$$

where Γ is the gamma function and

$$(Z+1)/Z = M_w/M_n \quad (17)$$

Then we convoluted eq 16 with eq 4 in combination with eq 7–12 to calculate the stress relaxation moduli at different Z values that solely determine the width of the MWD. The optimum Z value for each sample was determined by the best matching of the calculated and measured stress relaxation curves.

The $\mu_X(t)$ process is not sensitive to MWD. The contribution of $\mu_X(t)$ to the $G(t)$ curve is calculated according to eq 15 by using M_w for M. The $\mu_A(t)$ process is independent of MW (eq 6). The $G(t)$ curve in the $\mu_A(t)$ region is solely determined by the K value in eq 6 (denoted as K').

Because of its high modulus value, the glassy region of $G(t)$ is much affected by the compliance of the transducer, as shown in section III. The agreement between theory and experiment in the glassy region reported previously,[8] whereby the best value of N_e (see eq 6) could be determined, was an error due to negligence of the compliance effect of the transducer. No existing theory is available for analyzing $G(t)$ in the glassy region.

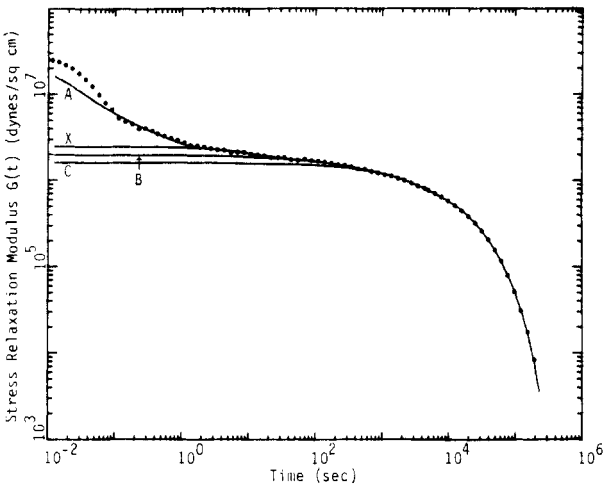

Figure 4. Comparison of the measured (···) and calculated stress relaxation modulus (—) for the F40 sample. Also shown are the separate contributions of the $\mu_A(t)$, $\mu_X(t)$, $\mu_B(t)$, and $\mu_C(t)$ processes.

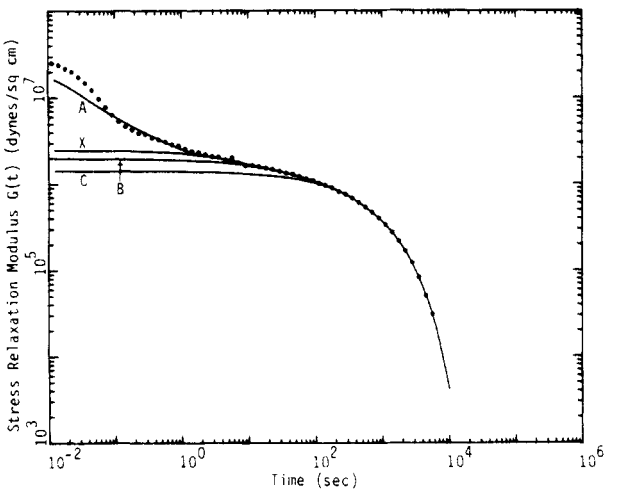

Figure 5. Same as Figure 4 for the NBS sample.

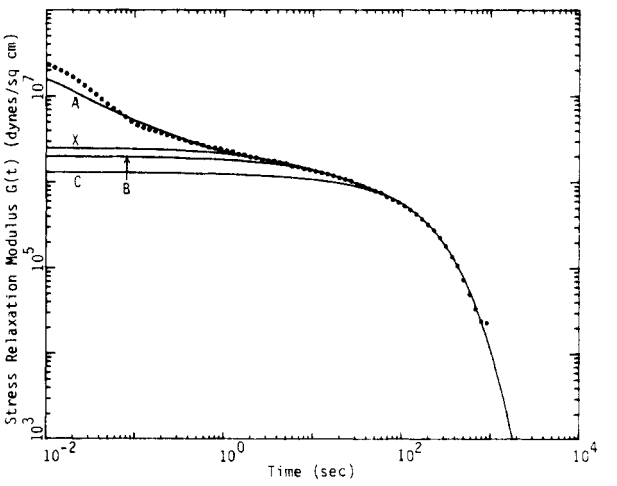

Figure 6. Same as Figure 4 for the L11 sample.

In the transition region (the $\mu_A(t)$ process region not affected by the glassy relaxation), the calculated $G(t)$ curve is very much independent of the N_e value as long as it is sufficiently large. Ten is a very reasonable number for N_e,[19,20] which we have used for the calculation of the $\mu_A(t)$ contribution in this study.

In the same way as reported previously,[8] three component MWD's are extracted from the stress relaxation curves for F40 and NBS by using a nonlinear least-squares fitting computer program.

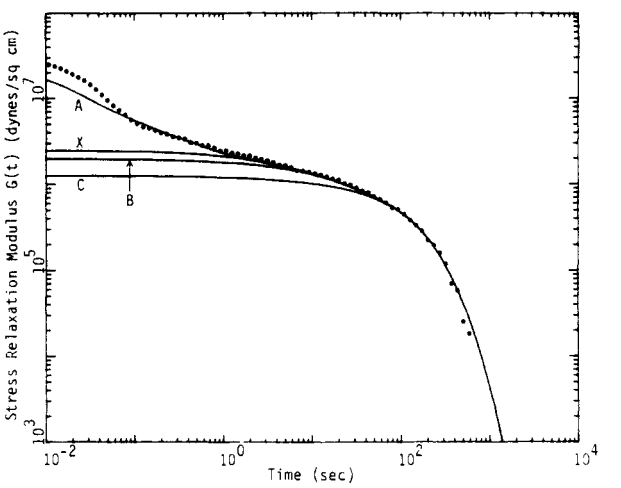

Figure 7. Same as Figure 4 for the F10 sample.

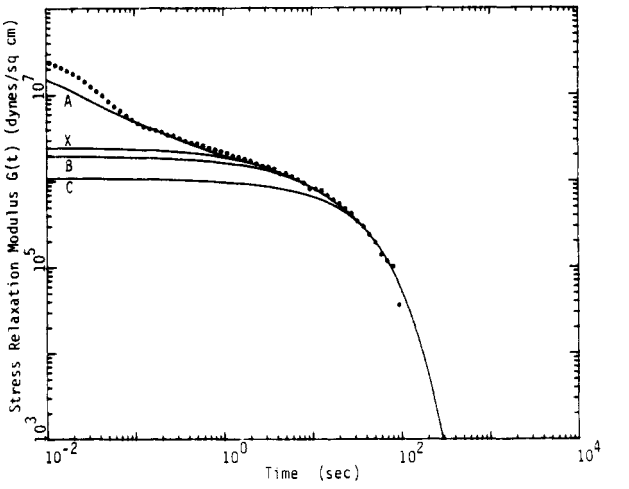

Figure 8. Same as Figure 4 for the P7 sample.

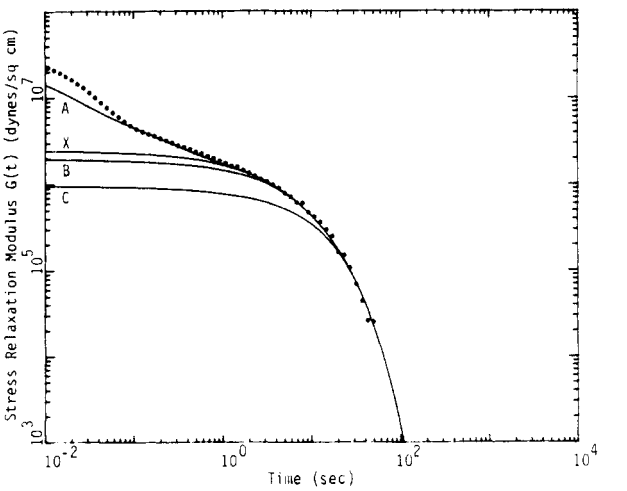

Figure 9. Same as Figure 4 for the P5 sample.

The calculated and measured stress relaxation curves are compared in Figures 4–13 for samples F40, NBS, L11, F10, P7, P5, F4, L3, P3, and F2, respectively. The M_e value used in all the line shape calculations is 13 500, corresponding to $G_N = 2 \times 10^6$ dyn/cm^2. The three-component MWD's extracted from the $G(t)$ line shapes of F40 and NBS through nonlinear least-squares fitting are shown in Figures 14 and 15. The M_w/M_n values of the three-components MWD's are 1.16 and 1.08 for F40 and NBS, respectively. The Schulz MWD's used to calculate $G(t)$'s for the rest of the samples are shown in Figure 16. Their M_w/M_n values range from 1.01 to 1.03, in good agreement

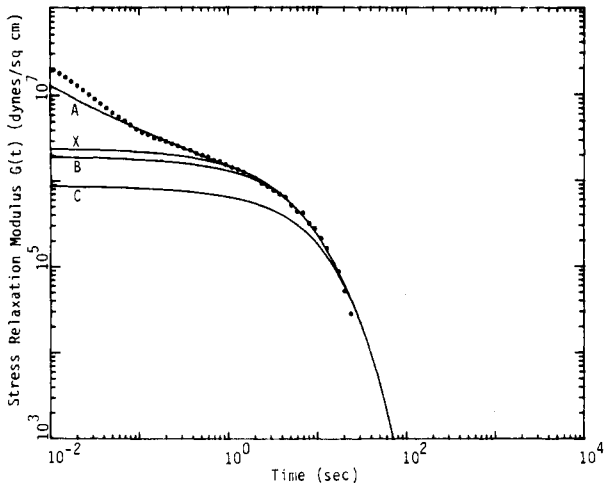

Figure 10. Same as Figure 4 for the F4 sample.

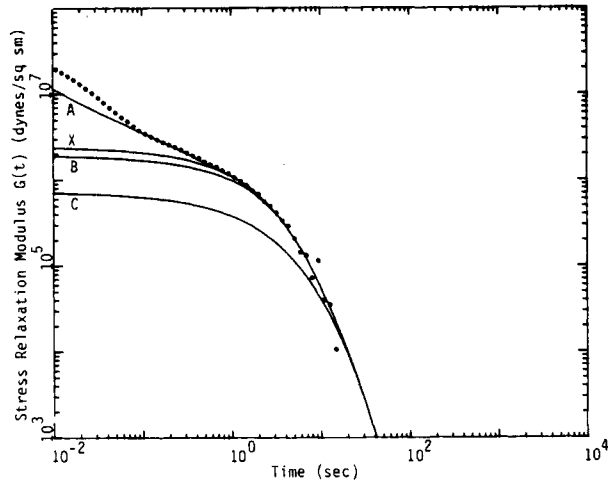

Figure 11. Same as Figure 4 for the L3 sample.

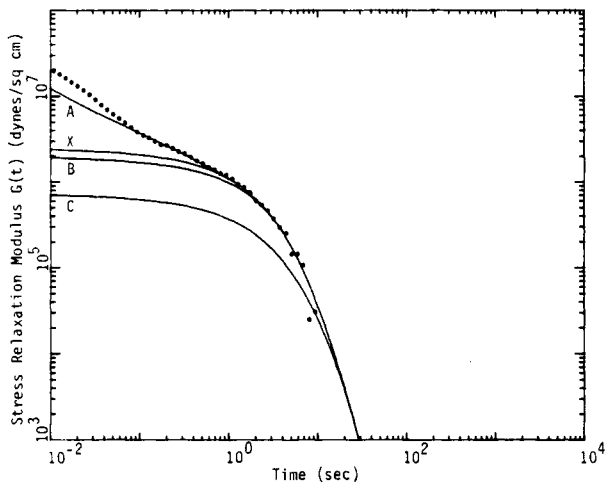

Figure 12. Same as Figure 4 for the P3 sample.

with the GPC values listed in Table I.

In the MW region of L11 to F2, the plateau region of the stress relaxation modulus has virtually disappeared. The line shape of $G(t)$ is so lack of a "corner" in the terminal region that if only the reptational process of Doi and Edwards is used to analyze $G(t)$ the MWD that can be extracted will be very much broader than it really is. In this MW region, the $\mu_B(t)$ process plays a very important role because of the following reasons: First, its relaxation strength, B, (eq 7) becomes of the same order of magnitude as that of the $\mu_C(t)$ process (eq 8). Second, the relaxation time τ_B becomes very close to the τ_C value. These effects

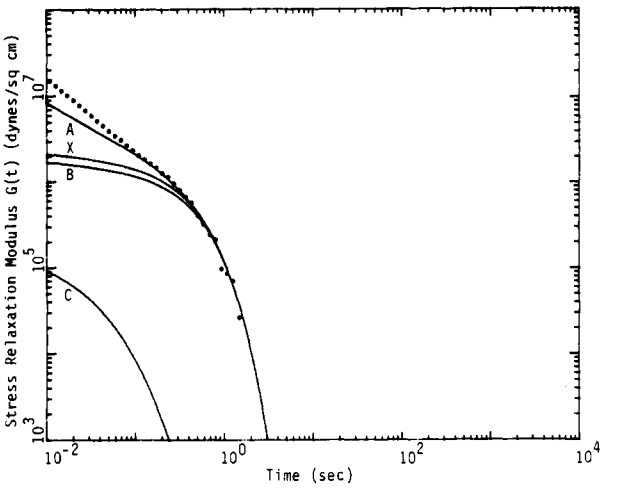

Figure 13. Same as Figure 4 for the F2 sample.

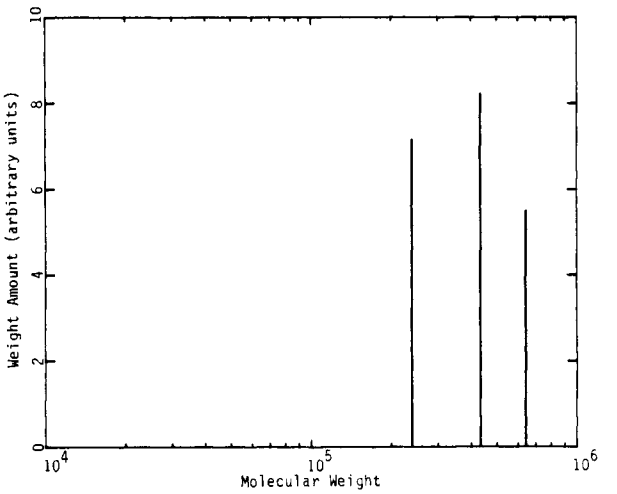

Figure 14. Three-component MWD that is extracted from the stress relaxation modulus of the F40 sample using a nonlinear least-squares fitting computer program (see the text and Figure 4).

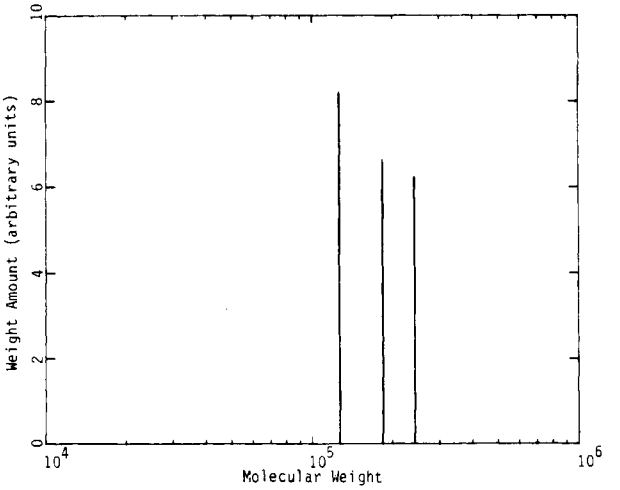

Figure 15. Same as Figure 14 for the NBS sample (see Figure 5).

are demonstrated by the separate contributions of the $\mu_B(t)$ and $\mu_C(t)$ processes shown in Figures 6–13.

By the inclusion of both the $\mu_B(t)$ and $\mu_C(t)$ processes in the $G(t)$ line shape analysis, the narrow MWD's as shown in Figure 16 can be extracted. The success of the line shape analysis in this medium- and low-MW region, where the modulus plateau is either nondistinct or absent,

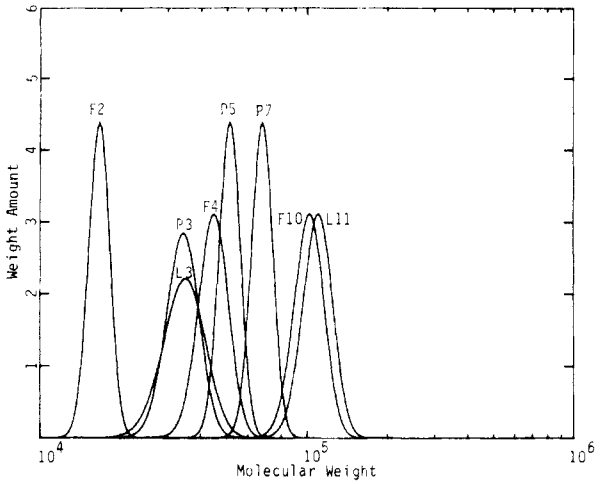

Figure 16. Normalized Schulz MWD's that are used to calculate the stress relaxation moduli of L11 (Z = 60), F10 (Z = 60), P7 (Z = 120), P5 (Z = 120), F4 (Z = 60), L3 (Z = 30), P3 (Z = 50), and F2 (Z = 120) (see Figures 6–13).

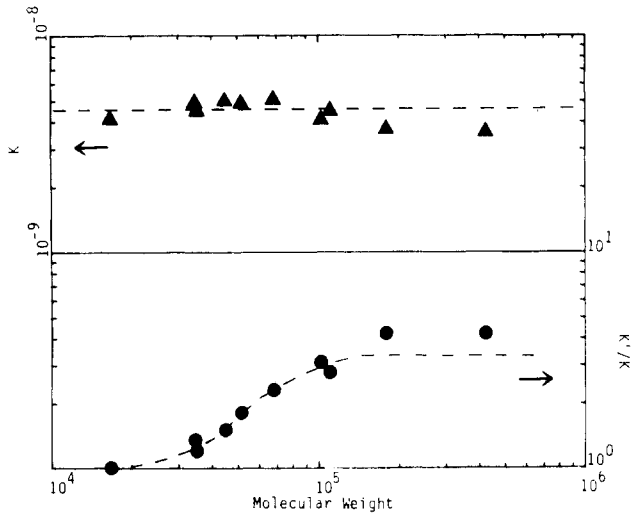

Figure 17. K and K'/K values as a function of MW that have been obtained from the line shape analysis of the measured $G(t)$'s. The reproducibility of the K values obtained from $G(t)$ measurements on different days is within 20%. To eliminate the effect of temperature drift from day to day, measurements of several different samples were made in the same day. Through overlapping results of different days, a small correction was made to the data values. The values shown here are the averages of several such corrected values.

strongly supports the proposed general theory.

Furthermore, the K values (see eq 10, 12, and 13) obtained for the different samples are independent of MW within experimental error, as shown in Figure 17. This strongly supports that eq 10 and 12 correctly give the MW dependence of τ_B and τ_C, respectively.

The K values of the F40 and NBS samples are about 30% lower than the average value of the rest of the samples (as indicated by the dashed line in Figure 17). This may be due to the error of the M_w value used in the calculation. A 30% error in the K value can be caused by less than 10% error of the M_w value (see eq 10 and 12). However, we believe that the accuracy of the M_w values of the studied samples is better than within 10%. The 30% lower values of the K constant for F40 and NBS are mainly due to the sensitivity of the $G(t)$ line shape to the MWD width at high MW and the low-MW tail that often exists in the high-MW samples.

To simplify the explanation for the effect of low-MW components to $G(t)$, one can assume that the sample consists of only two MW components. If the MW of the low-MW component is sufficiently low compared to the high-MW component, some of the tube stress associated with the high-MW component will relax in a time shorter than the reptation time of the high-MW component, as the low-MW molecules reptate away (disentangle) from the high-MW molecules (i.e., the tube renewal process). This phenomenon has been observed in our study of the blending law.[21] Thus, a small amount of the low-MW component can cause a steeper decline in the observed plateau region and reduce the sharpness of the "corner" in the terminal region. This effectively broadens the MWD that can be extracted from the $G(t)$ data. Because the modulus plateau is wider and its $\Delta t/\Delta G$ value is larger at higher MW, this effect is enhanced at high MW. The M_w/M_n value extracted from the $G(t)$ line shape of F40 is significantly increased artifically by the breadth of its MWD and the low-MW tail in the samples (see Figure 23). The large low-MW tail in the NBS sample (see Figure 24) has a similar effect. The M_w/M_n values of the three-component MWD's extracted from the $G(t)$ line shape analysis for F40 and NBS are greater than those of the rest of the samples, partly due to its intrinsic broader MWD and partly due to the described broadening effect. The linear additivity assumed in the three-component MWD used to analyze the $G(t)$ line shapes of these two samples is not strictly obeyed.

This tube-renewal effect caused by the low-MW components is not large and somewhat enhances the fast relaxation processes for F40 and NBS. As a result, the K value extracted from the line shape analysis of $G(t)$ is slightly smaller. This explanation is supported by the viscosity data obtained from integration over the measured $G(t)$ curves of the studied samples as reported in the accompanying paper (paper 3). The obtained viscosity values are in very good agreement with the theoretical curve over the entire MW range. In other words, the viscosities of F40 and NBS do not show a 30% deficiency as their corresponding K values. This seeming paradox can be resolved by the above explanation, assuming that within the MWD range of our current interest ($M_w/M_n < 1.2$), the experimental viscosity value is basically a function of M_w only and independent of MWD. An equivalent explanation is as follows: We can approximate the general linear viscoelastic theory by the Doi–Edwards theory and still account for the dominant part of the MW dependence of the zeroshear viscosity. Assuming the linear additivity law applied to the Doi–Edwards theory, Graessley[22] showed that $\eta_0 \propto M_w M_z M_{z+1}$ instead of $\eta_0 \propto M_w^3$. Since $M_{z+1} > M_z > M_w$, in order to make $\eta_0 \propto M_w^3$ (corresponding to $\eta_0 \propto M_w^{3.4}$ as observed experimentally), the K value, which is obtained from the forced computer fitting to the $G(t)$ line shape in terms of the three-component MWD (for the cases of the F40 and NBS samples), has to be smaller than it would be for ideal monodispersity.

Very significantly, the K value remains quite independent of MW to the MW value as low as 16 700 (M_w of the F2 sample), as shown in Figure 17. At M_w = 16 700, the K value being slightly lower than the average value may be due to slightly larger free volume at this low MW. Overall, the change of free volume or T_g with MW in the MW region $10M_e$–M_e does not affect the K value but affects the K' value (the K value of eq 6) greatly.

As explained above, because of the presence of the glassy relaxation process in the short-time region, the relaxation line shape cannot be used to determine the N_e value in the $\mu_A(t)$ process. However, the matching of experimental and calculated values in the region of low motional modes of

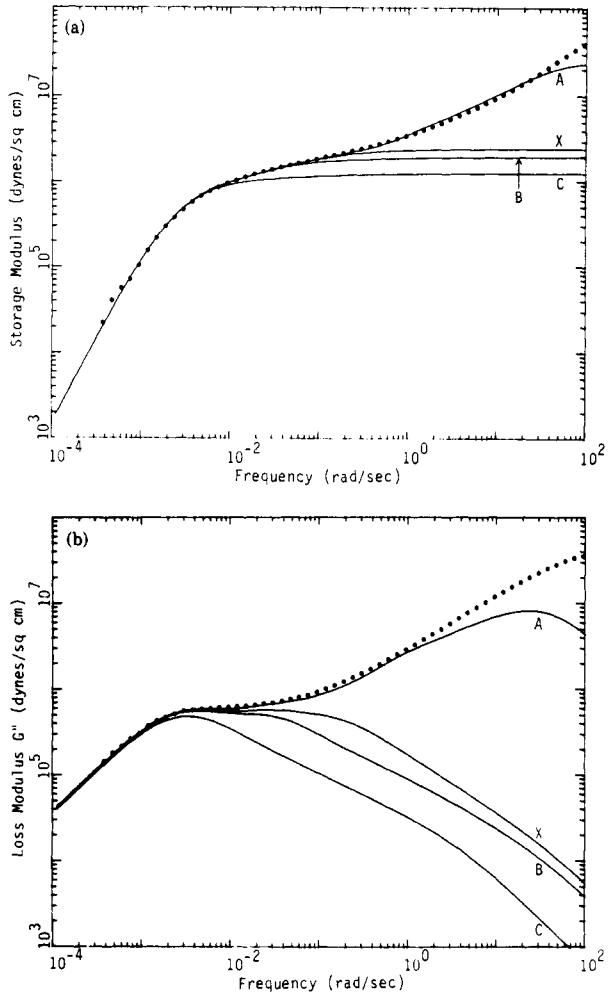

Figure 18. (a) Comparison of the measured (···) and calculated (—) storage moduli of F10. Also shown are the separate contributions of the $\mu_A(t)$, $\mu_X(t)$, $\mu_B(t)$, and $\mu_C(t)$ processes. (b) Comparison of the measured (···) and calculated (—) loss moduli of F10. Also shown are the separate contributions of the $\mu_A(t)$, $\mu_X(t)$, $\mu_B(t)$, and $\mu_C(t)$ processes.

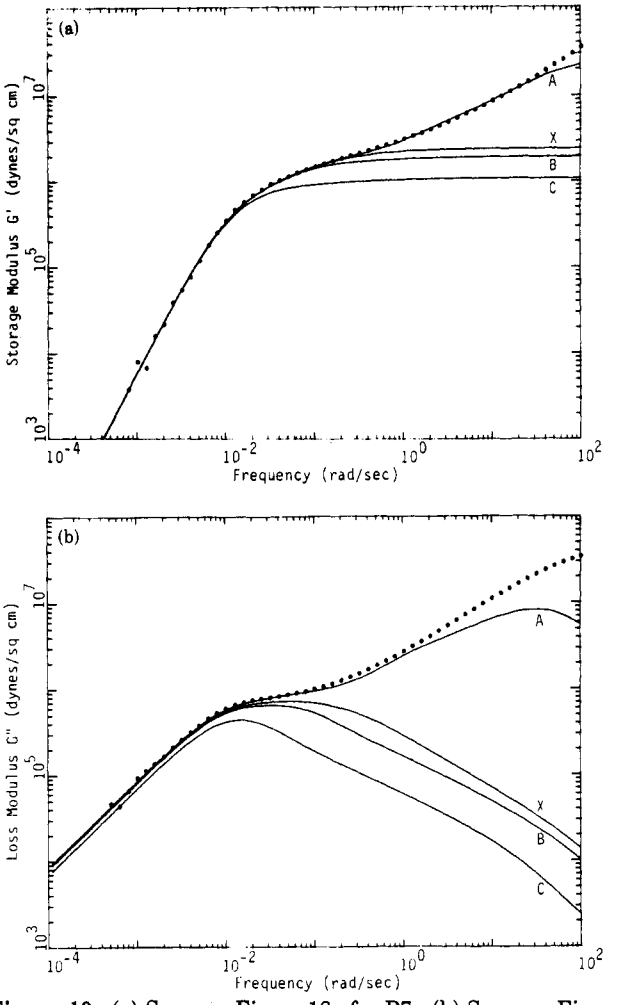

Figure 19. (a) Same as Figure 18a for P7. (b) Same as Figure 18b for P7.

$\mu_A(t)$ is sufficient to determine the K' value. The K' values are obtained from fitting the experimental $G(t)$ values in the transition region to the $\mu_A(t)$ process (eq 4–6) shown by its contributions in Figures 4–13.

As shown in Figure 17, in the high-MW region, the K'/K value is independent of MW and has a value of about 4.2. At MW $\sim$ 140 000, it begins to decrease with decreasing MW and reaches a limiting value of 1 at low MW (MW $\sim M_e(+)$).

It has been proposed[8] that for $K'/K > 1$, the friction coefficient for the polymer chain segment to move in the direction perpendicular to the chain contour is higher than that along the chain contour. This is a reasonable explanation, if we consider that a certain local extra free volume is associated with the polymer chain end. This extra free volume is always available to the $\mu_B(t)$ and $\mu_C(t)$ processes, in which the polymer chain moves along the chain contour. On the other hand, the portion of this extra free volume available to the $\mu_A(t)$ process of a polymer chain depends on the concentration of free chain ends of polymer molecules surrounding it. Thus, the K' value extracted from the $\mu_A(t)$ process is MW dependent. Furthermore, the K'/K value approaching the value 1 at low MW supports this explanation.

The K'/K values of F40 and NBS become 3.3 after correcting for the 30% underestimation of their K values. The corrected K'/K value in the high-MW region, where K'/K is basically independent of MW, is indicated by the dashed line in Figure 17.

The contributions of the $\mu_X(t)$ process to the total $G(t)$ line shapes shown in Figures 4–13 are calculated with eq 15 for the MW dependence of its relaxation time τ_X. By the combination of a scaling argument and the results of $G(t)$ line shape analysis, the form and coefficient of eq 15 were determined in paper 1. The validity of eq 15 is further confirmed by the close fitness of the calculated $\mu_X(t)$ contributions to the measured $G(t)$ line shapes of all the samples studied in this report.

V. Storage and Loss Moduli

To confirm our line shape analysis of $G(t)$, especially in the MW region where the modulus plateau is either nondistinct or absent, the storage and loss moduli, $G'(\omega)$ and $G''(\omega)$, of F10, P7, P5, F4, and F2 are measured and compared with those calculated from eq 4 in combination with eq 5–17. The Z values used in the Schulz MWD for these samples are the same as those used in the calculation of their $G(t)$ curves (Figures 7–10 and 13). For calculating the $G'(\omega)$ and $G''(\omega)$ values using the linear viscoelastic relations

$$G'(\omega) = \omega \int_0^\infty G(t) \sin \omega t \, dt \tag{18}$$

$$G''(\omega) = \omega \int_0^\infty G(t) \cos \omega t \, dt \tag{19}$$

a computer program containing the single and coupled

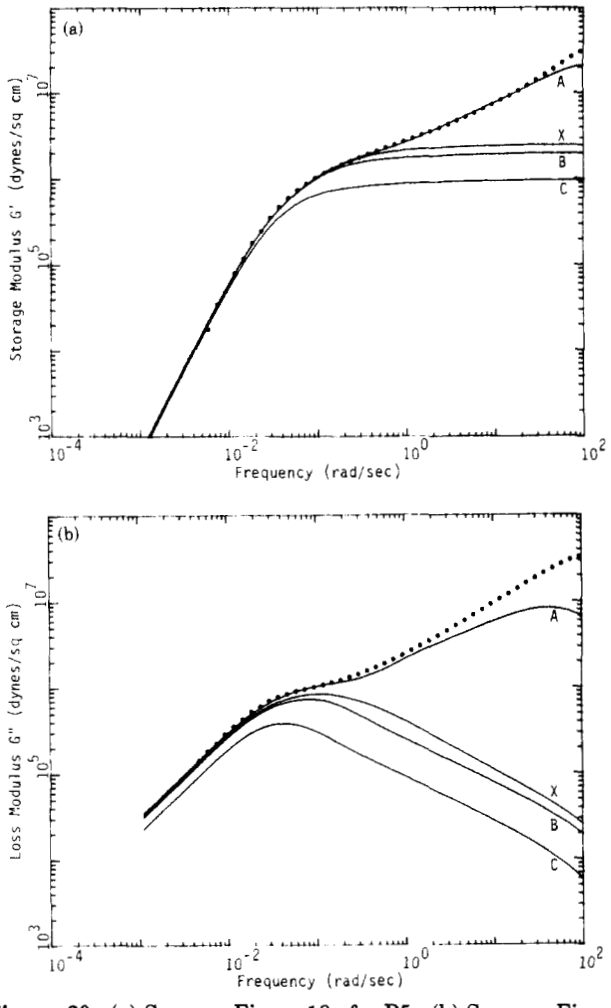

Figure 20. (a) Same as Figure 18a for P5. (b) Same as Figure 18b for P5.

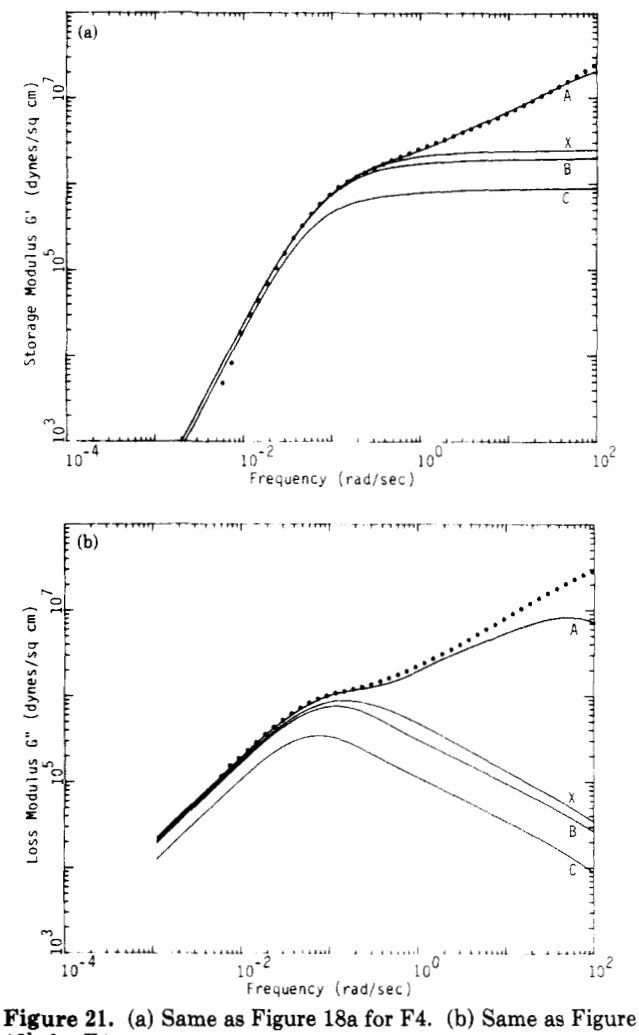

Figure 21. (a) Same as Figure 18a for F4. (b) Same as Figure 18b for F4.

Fourier transformed terms of the $\mu_A(t)$, $\mu_X(t)$, $\mu_B(t)$, and $\mu_C(t)$ processes up to $P = 9$ for $\mu_A(t)$ and $P = 35$ for $\mu_B(t)$ and $\mu_C(t)$ (see eq 5, 9, and 11) was used. This is a more accurate and efficient way of calculating $G'(\omega)$ and $G''(\omega)$ than a direct numerical Fourier transform from the calculated $G(t)$, since the calculation extends over several decades of frequencies.

The measured and calculated $G'(\omega)$ and $G''(\omega)$ of F10, P7, P5, F4, and F2 are compared in Figures 18–22, respectively. In the comparison, the experimental results are shifted to fit to the theoretical curves calculated with $K = 1 \times 10^{-8}$. The K'/K values used for these samples are those shown in Figure 17. In each of these $G'(\omega)$ and $G''(\omega)$ figures, the separate contributions of the $\mu_A(t)$, $\mu_X(t)$, $\mu_B(t)$, and $\mu_C(t)$ processes are also shown.

For the storage modulus, $G'(\omega)$, the agreements between theory and experiment for all the samples are very good over the entire frequency range, except the expected difference in the high-frequency glassy region. In the case of the loss modulus, $G''(\omega)$, good agreements between theory and experiment are observed up to the modulus value of $\sim 1 \times 10^6$ dyn/cm^2 for all the samples. Beyond $G''(\omega) \sim 1 \times 10^6$ dyn/cm^2, the measured $G''(\omega)$ values rise faster than the theoretical curves and cross the measured $G'(\omega)$ values at $3–5 \times 10^6$ dyn/cm^2, while the theoretical $G'(\omega)$ and $G''(\omega)$ curves do not cross in this high-frequency or high-modulus region. The difference of $G''(\omega)$ values between theory and experiment in this region is due to the glassy relaxation process, which is not included in the general stress relaxation form (eq 4). The effect of the glassy relaxation process on the $G'(\omega)$ values is limited in the high-frequency region where it occurs (i.e., the reciprocal of its relaxation time). On the other hand, the effect of the glassy relaxation process on the $G''(\omega)$ values extends to lower frequencies, because of the mathematical form of transforming $G(t)$ to $G''(\omega)$ (eq 19).

As M_w decreases, the contribution of $\mu_C(t)$ to the total $G'(\omega)$ and $G''(\omega)$ decreases while that of $\mu_B(t)$ increases. Simultaneously, the relaxation time μ_B becomes closer to τ_C and eventually becomes larger than τ_C at $M_w \sim M_c$. Furthermore, at $M_w \sim M_c$, both $\mu_B(t)$ and $\mu_C(t)$ become very close to $\mu_A(t)$. All these effects cause the gradual disappearance of the modulus plateau on $G'(\omega)$ and the modulus hump in the terminal region of $G''(\omega)$ with decreasing MW.

Noteworthy is the minor role played by the $\mu_C(t)$ process for the F2 sample, whose M_w is between M_c and M_e. In the low-MW region, $M_c > \text{MW} > M_e$, the polymer molecule behaves like an "anisotropic" Rouse-like chain—with the Rouse-like motions ($\mu_B(t)$) along chain contour direction being different from the Rouse motion ($\mu_A(t)$) perpendicular to the chain contour.

VI. Discussion and Conclusion

In paper 1, a general linear viscoelastic theory was proposed and three nearly monodisperse polystyrene samples with MW's ranging from 186 000 to 775 000 were studied for comparison with the general theory. In this report, the MW range is extended as low as 16 700, overlapping the previous MW range from ~179 000 to 422 000. It is found that the proposed general theory is applicable

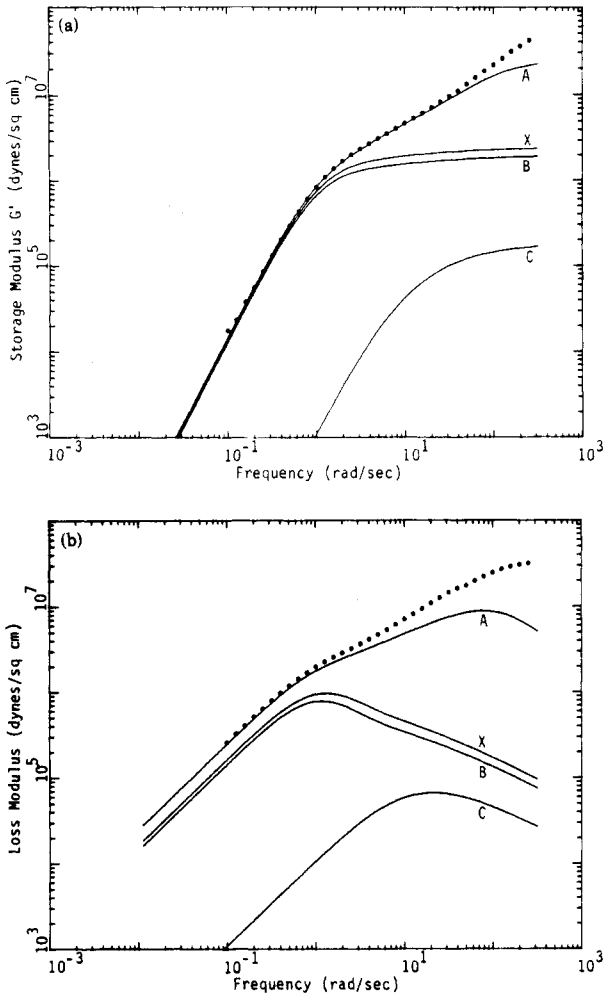

Figure 22. (a) Same as Figure 18a for F2. (b) Same as Figure 18b for F2.

over the entire MW range that has been studied.

While the rates of stress relaxations of the samples studied in this report range over five decades (see Figure 3), the K values extracted from the stress relaxation line shape analysis is independent of MW. This is a very significant result, which strongly supports that the separation of $G(t)$ in the long-time region into the $\mu_B(t)$ and $\mu_C(t)$ processes, as described by eq 9 and 11, respectively, is valid and that eq 10 and 12 have the correct form for the MW dependence of τ_B and τ_C. The constraint effect due to chain entangelements as described by the proposed general theory persists to the low-MW regions M_c > MW > M_e.

In the MW region where the modulus plateau on $G(t)$ and $G'(\omega)$ and the modulus hump on $G''(\omega)$ are either nondistinct or absent, the line shapes of the linear viscoelastic spectra are well described by the convolution of the general stress relaxation form with the Schulz MWD. The Z value, which determines the width of the MWD, is the only adjustable parameter. The M_w/M_n values extracted from the line shape analysis are in good agreement with those of GPC.

The line shape analysis of $G(t)$, $G'(\omega)$, and $G''(\omega)$ shows the increasingly important role played by $\mu_B(t)$ relative to $\mu_C(t)$ as the MW decreases. Eventually both $\mu_B(t)$ and $\mu_C(t)$ become very close to $\mu_A(t)$. These effects cause the modulus plateau to disappear gradually with decreasing MW. The increasing importance of $\mu_B(t)$ at low MW and eq 12 (corrected for the chain-length fluctuation effect) are the major factors that cause the difference between the observed MW dependence of viscosity ($\eta_0 \propto M^{3.4}$) and the

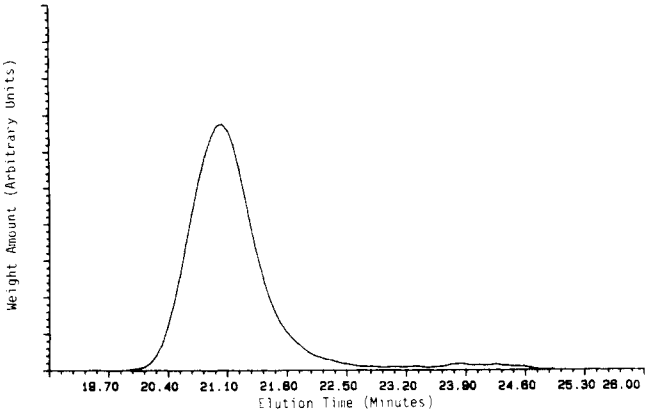

Figure 23. GPC spectrum of the F40 sample.

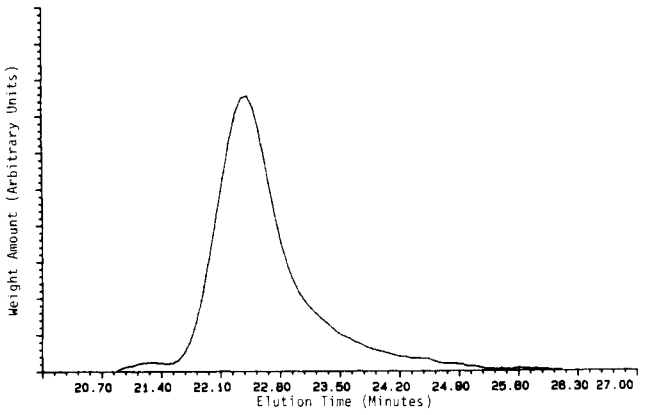

Figure 24. GPC spectrum of the NBS sample.

prediction of the reptation chain model ($\eta_0 \propto M^3$), which will be analyzed in more detail in the accompanying paper.

The general linear viscoelastic theory was developed by assuming that the constraint release effect is negligible for ideal monodispersity or extremely narrow MWD. The good agreement between theory and experiment over the entire MW range studied confirms the validity of this assumption. However, we have observed some effect caused by the constraint release due to the low-MW components in the F40 and NBS samples. This effect causes about 30% deficiency of the K values obtained from the $G(t)$ line shape analysis for the F40 and NBS samples.

The $\mu_X(t)$ process implicitly exists in the Doi–Edwards theory. The MW dependence of its relaxation time is given by eq 15. For all the studied samples, the calculated $\mu_X(t)$ contributions closely fit the measured $G(t)$ line shapes. These quantitative agreements further confirm the form and the coefficient of eq 15, which had been determined in paper 1.

From the data analysis in the $\mu_A(t)$ region, a very interesting and significant phenomenon, that the K' value decreases with decreasing MW in the MW region MW < $10M_e$, is discovered. An explanation for this observed phenomenon is given. Consistent with the explanation is the fact that T_g (related to free volume and friction coefficient) is slightly affected by the decrease of MW in the same MW region. Since K' is the only physical quantity related to friction coefficient that changes with MW, it is strongly suggested that the change of K' with MW is directly related to the change of T_g or free volume with MW. In the accompanying paper, how this effect is related to the T_g correction for viscosity will be analyzed.

Acknowledgment. The author thanks Dr. L. J. Fetters of Exxon Research and Engineering Co. for providing two of the studied samples.

Appendix

The measured GPC spectra of the F40 and NBS samples are shown in Figures 23 and 24, respectively. The F40 sample has a width at half-height slightly greater than that of NBS, and both samples have a low-MW tail. See the text for their effects on the $G(t)$ line shape.

References and Notes

(1) Ferry, J. D. "Viscoelastic Properties of Polymers", 3rd ed.; Wiley: New York, 1980.
(2) Graessley, W. W. *Adv. Polym. Sci.* **1974**, *16*, 1.
(3) de Gennes, P.-G. *J. Chem. Phys.* **1971**, *55*, 572.
(4) Doi, M.; Edwards, S. F. *J. Chem. Soc., Faraday Trans. 2* **1978**, *74*, 1789.
(5) Doi, M.; Edwards, S. F. *J. Chem. Soc., Faraday Trans. 2* **1978**, *74*, 1802.
(6) Doi, M.; Edwards, S. F. *J. Chem. Soc., Faraday Trans. 2* **1978**, *74*, 1818.
(7) Doi, M.; Edwards, S. F. *J. Chem. Soc., Faraday Trans. 2* **1979**, *75*, 38.
(8) Lin, Y.-H. *Macrocmolecules* **1984**, *17*, 2846.
(9) Mooney, M. *J. Polym. Sci.* **1959**, *34*, 599.
(10) Treloar, L. R. G. "The Physics of Rubber Elasticity", 2nd ed.; Oxford University Press: London, 1958.
(11) Mark, J. E. *J. Am. Chem. Soc.* **1970**, *92*, 7252.
(12) Lin, Y.-H. J. Rheol. **1984**, *28*, 1.
(13) Osaki, K.; Kurate, M. *Macromolecules* **1980**, *13*, 671.
(14) Vrentas, C. M.; Graessley, W. W. *J. Rheol.* **1982**, *26*, 359.
(15) Onogi, S.; Masuda, T.; Kitgawa, K. *Macromolecules* **1970**, *3*, 109.
(16) Boyer, R. F. *Rubber Chem. Technol.* **1963**, *36*, 1303.
(17) Schulz, G. V. *Z. Physik. Chem., Abst. B* **1939**, *43*, 25.
(18) Tung, L. H. "Polymer Fractionation"; Cantow, M. J. R., Ed.; Academic: New York, 1967.
(19) Akcasu, A. Z.; Han, C. C. *Macromolecules* **1979**, *12*, 276.
(20) Osaki, K.; Schrag, J. L. *Polym. J. (Tokyo)* **1971**, *2*, 541.
(21) Lin, Y.-H., unpublished results. The blending law can be basically described by the following stress relaxation function for a blend system consisting of two monodisperse components which are far apart:

$$G(t) = G_N W_1[B_1\mu_B(t/\tau_{B1}) + C_1\mu_C(t/\tau_{C1})] + G_N W_2[W_1 T(t) + W_2][B_2\mu_B(t/\tau_{B2}) + C_2\mu_C(t/\tau_{C2})]$$

where W_1 and W_2 are the weight fractions of the low- and high-MW components, respectively, and $T(t)$ is a decaying function (for the tube-renewal process) with a characteristic time τ_T which is larger than the τ_{C1} value by about an order of magnitude. From analyzing the stress relaxation line shapes of nearly monodisperse MWD samples and the blend systems consisting of two components of such narrow MWD, it is suggested that the tube decaying function $T(t)$ for ideal monodispersity should be flat for a period $\tau_T \gg \tau_C$ and then decline quickly; i.e., the tube renewal process is negligible for ideal monodispersity. In a system where the high MW is 775 000 (the F80 polystyrene sample of TSK) and the low MW is 179 000 (the NBS sample), the τ_{C2} value is reduced to $0.85\tau_{C2}^0$ (τ_{C2}^0 is the τ_{C2} for $W_1 = 0$) at $W_1 = 0.25$, $0.7\tau_{C2}^0$ at $W_1 = 0.5$, and $0.5\tau_{C2}^0$ at $W_1 = 0.75$. With decreasing MW of the low-MW component, the effect of W_1 on the reduction of τ_{C2} increases. If the low MW is greater than ~400 000 estimated from extrapolation, τ_{C2} of F80 should not be reduced at $W_1 = 0.5$ (i.e., $\tau_{C2} = \tau_{C2}^0$). The physical meaning of the above equation for a blend system will be explained in detail in a future publication.
(22) Graessley, W. W. *J. Polym. Sci., Polym. Phys. Ed.* **1980**, *18*, 27.

Comparison of Experiment and the Proposed General Linear Viscoelastic Theory. 3. Zero-Shear Viscosity and Steady-State Compliance

Y.-H. Lin

Exxon Chemical Company, Plastics Technology Center, Baytown, Texas 77522.

Received March 26, 1985

ABSTRACT: It was shown that the proposed general linear viscoelastic theory explained the molecular weight (MW) dependence of the zero-shear viscosity ($\eta_0 \propto M^{3.4}$ above M_c, $\eta_0 \propto M$ below M_c), the steady-state compliance, and the transition points M_c and M_c'. To do so, some information extracted from the short-time viscoelastic relaxation data in the MW region much higher than M_c was used. The reason the calculated and measured MW dependences of η_0 in the low-MW region agree so well was not evident. On the basis of the new insights obtained from the line shape analysis of the stress relaxation moduli reported in the accompanying report (paper 2), an explanation is given. Furthermore, it is shown that the proposed general linear viscoelastic theory is applicable above M_e, while the Rouse theory is applicable just below M_e. The transition point appears rather sharp. The result suggests that as far as the free volume distribution on the polymer chain is concerned, there is a "phase" transition point at M_e(+) from "isotropic" to "anisotropic".

I. Introduction

Chain entanglement plays a very important role in the viscoelastic properties of concentrated polymer systems. One well-known example is the observed molecular weight (MW) dependence of the zero-shear viscosity $\eta_0 \propto M^{3.4}$, above the critical molecular weight (MW), M_c.[1,2] Empirically, the value of M_c is about twice the entanglement MW, M_e, which can be determined from the plateau modulus. Below M_c the viscosity increases linearly with M, as predicted by the Rouse theory. Similarly, the measured steady-state compliance J_e increases linearly with MW below M_c and is independent of MW above M_c'.[1,2]

The reptation model[3-7] predicted that the zero-shear viscosity scaled with MW as $\eta_0 \propto M^3$. In paper 1,[8] a general linear viscoelastic theory was developed from modifying the Doi–Edwards theory.[4-7] It was shown that the general theory explained the MW dependence of η_0 and J_e and the transition points M_c and M_c'. To do so, some information extracted from the short-time viscoelastic relaxation data in the MW region much higher than M_c was used. The reason the calculated and measured MW dependence of η_0 in the low-MW region agree so well was not evident.

In paper 2,[9] the viscoelastic relaxation spectra of narrow MWD polystyrene samples over a wide range of MW

0024-9297/86/2219-0168$01.50/0